J|A|C|S
ARTICLES
Published on Web 06/14/2003

In Silico Studies of the Mechanism of Methanol Oxidation by Quinoprotein Methanol Dehydrogenase

Swarnalatha Y. Reddy and Thomas C. Bruice*

Contribution from the Department of Chemistry and Biochemistry, University of California−Santa Barbara, Santa Barbara, California 93106

Received January 29, 2003; E-mail: tcbruice@bioorganic.ucsb.edu

Abstract: The mechanism of bacterial methanol dehydrogenase involves hydride equivalent transfer from substrate to the ortho-quinone PQQ to provide a C5-reduced intermediate that subsequently rearranges to the hydroquinone $PQQH_2$. We have studied the PQQ reduction by molecular dynamic (MD) simulations in aqueous solution. Among the five simulated structures, either Asp297 or Glu171 or both are ionized. Reasonable structures are obtained only when both carboxyl groups are ionized. This is not unexpected since the kinetic pH optimum is 9.0. In the structure of the enzyme·PQQ·$HOCH_3$ complex, the hydrogen bonded Glu171$-CO_2^-\cdots$H$-OCH_3$ is in a position to act as a general base catalyst for hydride equivalent transfer to C5 of PQQ. We thus suggest that Glu171 plays the role of general base catalyst in PQQ reduction rather than Asp297 as previously suggested. The reduction is assisted by Arg324, which hydrogen bonds to the ortho-quinone moiety of PQQ. The rearrangement of the C5-reduced intermediate to provide hydroquinone $PQQH_2$ is also assisted by proton abstraction by Glu171$-CO_2^-$ and the continuous hydrogen bonding of Arg324 throughout the entire reaction. These features as well as the mapping of the channel for substrate and water into the active site entrance are the observations of major importance.

Introduction

The quinoproteins methanol dehydrogenase (MDH) and glucose dehydrogenase (GDH) are bacterial enzymes[1−5] that require the ortho-quinone PQQ as a cofactor.[6,7] The chemistry of 2,7,9-tricarboxy-1*H*-pyrrolo [2,3-f]-quinoline-4,5-dione (PQQ) and the functions of PQQ have been well studied.[2,8−11] Both enzymes require Ca^{2+} for catalytic activity.[4,12−14] The subject of this study is MDH, a soluble periplasmic protein that uses acidic cytochrome c_L as the physiological electron acceptor.[15] After oxidation of methanol, MDH releases product formaldehyde, followed by two sequential single-electron transfers to cytochrome c_L. MDH consists of two dimers, consisting each of one light and one heavy subunit.[16−19] The two dimers are related by a local 2-fold symmetry axis, with heavy subunits in contact across the 2-fold axis.

Two mechanisms have been proposed for the enzyme activity of MDH. The first (Scheme 1) involves a general base-catalyzed proton abstraction from the methanol in concert with hydride ion transfer from the putative methoxide to the quinone carbonyl carbon C5 of PQQ and subsequent tautomerization to the hydroquinone $PQQH_2$.[5,18,20,21] The second mechanism involves the nucleophilic addition of the putative methoxide to the carbonyl C5 of PQQ to form a hemiketal intermediate, followed by an intramolecular retro-ene reaction.[5,18,22−25]

The hydride transfer mechanism finds support in the determination of the structure of the immediate PQQ reduction product (**II** of Scheme 1) by X-ray crystallography.[19] Also, the arrangement of glucose and PQQ in the active site of the GDH crystal structure favors the hydride transfer mechanism for glucose oxidation.[26−28]

* Author for correspondence. Phone: 805-893-2044. Fax: 805-893-2229.

(1) Anthony, C. *Adv. Microb. Physiol.* **1986**, *27*, 113.
(2) Duine, J. A. *Eur. J. Biochem.* **1991**, *200*, 271.
(3) Davidson, V. L. Methylamine Dehydrogenase. In *Principles and Applications of Quinoproteins*; Davidson, V. L., Ed.; Marcel Dekker: New York, 1993; p 73.
(4) Olsthoorn, A. J.; Duine, A. J. *Arch. Biochem. Biophys.* **1996**, *336*, 42.
(5) Anthony, C. *Biochem. J.* **1996**, *320*, 697.
(6) Salisbury, S. A.; Forrest, H. S.; Cruse, W. B. T.; Kennard, O. *Nature* **1979**, *280*, 843.
(7) Duine, J. A.; Frank, J., Jr. *Biochem. J.* **1980**, *187*, 213.
(8) Anthony, C.; Zatman, L. J. *Biochem J.* **1967**, *104*, 960.
(9) Eckert, T. S.; Bruice, T. C.; Gainor, J. A.; Weinreb, S. M. *Proc. Natl. Acad. Sci. U.S.A.* **1982**, *79*, 2533.
(10) Eckert, T. S.; Bruice, T. C. *J. Am. Chem. Soc.* **1983**, *105*, 4431.
(11) Rodriguez, E. J.; Bruice, T. C. *J. Am. Chem. Soc.* **1989**, *111*, 7947.
(12) Adachi, O.; Matsushita, K.; Shinagawa, E.; Ameyama, M. *Agric. Biol. Chem.* **1990**, *54*, 2833.
(13) Richardson, I. W.; Anthony, C. *Biochem J.* **1992**, *287*, 709.
(14) White, S.; Boyd, G.; Mathews, F. S.; Xia, Z.-x.; Dai, W.-w.; Zhang, Y.-f.; Davidson, V. L. *Biochemistry* **1993**, *32*, 12955.
(15) Anthony, C. *Biochim. Biophys. Acta* **1992**, *1099*, 1.
(16) Ghosh, M.; Anthony, C.; Harlos, K.; Goodwin, M. G.; Blake, C. C. F. *Structure* **1995**, *3*, 177.
(17) Xia, Z.-x.; Dai, W.-w.; Zhang, Y.-f.; White, S. A.; Boyd, G. D.; Mathews, F. S. *J. Mol. Biol.* **1996**, *259*, 480.
(18) Xia, Z.-x.; He, Y.-n.; Dai, W.-w.; White, S. A.; Boyd, G. D.; Mathews, F. S. *Biochemistry* **1999**, *38*, 1214.
(19) Zheng, Y.-J.; Xia, Z.-x.; Chen, Z.-w.; Mathews, F. S.; Bruice, T. C. *Proc. Natl. Acad. Sci. U.S.A.* **2001**, *98*, 432.
(20) Zheng, Y.-J.; Bruice, T. C. *Proc. Natl. Acad. Sci. U.S.A.* **1997**, *94*, 11881.
(21) Afolabi, P. R.; Mohammed, F.; Amaratunga, K.; Majekodunmi, O.; Dales, S. L.; Gill, R.; Thompson, D.; Cooper, J. B.; Wood, S. P.; Goodwin, P. M.; Anthony, C. *Biochemistry* **2001**, *40*, 9799.
(22) Dekker, R. H.; Duine, J. A.; Frank, J.; Eugene, J. P.; Verwiel, J.; Westerling, J. *Eur. J. Biochem.* **1982**, *125*, 69.
(23) Frank, J.; Vankrimpen, S. H.; Verwiel, P. E. J.; Jongejan, J. A.; Mulder, A. C.; Duine, J. A. *Eur. J. Biochem.* **1989**, *184*, 187.
(24) Itoh, S.; Ogino, M.; Fukui, Y.; Murao, H.; Komatsu, M.; Ohshiro, Y.; Inoue, T.; Kai, Y.; Kasai, N. *J. Am. Chem. Soc.* **1993**, *115*, 9960.
(25) Itoh, S.; Kawakami, H.; Fukuzumi, S. *Biochemistry* **1998**, *37*, 6562.
(26) Oubrie, A.; Rozeboom, H. J.; Kalk, K. H.; Olsthoorn, A. J. J.; Duine, J. A.; Dijkstra, B. W. *EMBO J.* **1999**, *18*, 5187.

Scheme 1 [5,18,20,21]

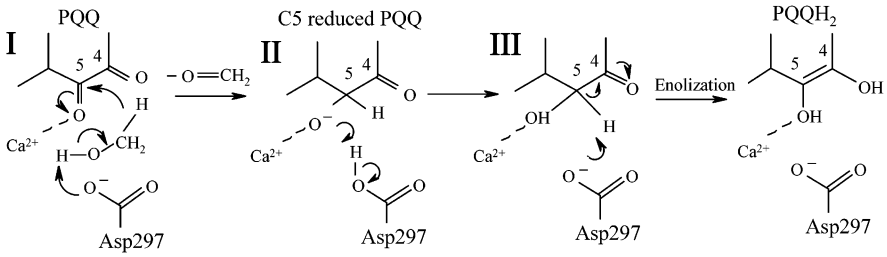

Chart 1

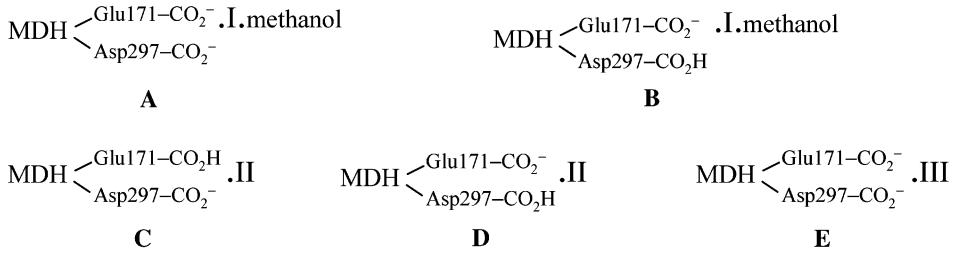

Recently, we compared the crystal and molecular dynamics (MD) structures[29] of MDH with the C5-reduced intermediate of PQQ (**II** of Scheme 1) at the active site. In this report, we expand the study of the ground state and intermediate structures of Scheme 1 using MD strategy. Due to the pivotal role suggested for the amino acid residues Glu171 and Asp297, we have studied structures in which the carboxylate side chains of these residues are either in $-CO_2^-$ or in $-CO_2H$ forms. The structures studied are given in Chart 1 (structure **D** is from a previous study[29]). At the pH optimum of 9 for activity, structures **A** and **E** represent stable entities, while **C** and **D** represent transient entities. A major contribution of the study represents the establishment of structures **A** and **E**.

Methods

Modeling of the Cofactor. The starting structure (1.9 Å resolution) of the PQQ containing MDH, a heterotetramer with 571 and 57 residues in each of the two heavy and two light subunits, respectively, was taken from the entry of 1G72 of the Protein Data Bank.[19] In the crystal structure, the cofactor has a tetrahedral configuration at the C5 atom, which is inferred to be the C5-reduced intermediate of PQQ. For construction of PQQ·methanol-bound enzyme complexes, the geometry of PQQ (characteristic of quinone carbonyl carbon C5 to be planar) from another crystal structure (PDB code 4AAH)[17] was docked in the active site of both the heavy subunits of MDH using the program SYBYL.[30] The partial atomic charges of the PQQ in the presence of the Ca^{2+} ion were obtained by means of quantum chemical calculations using Gaussian 98.[31] The PQQ structure with 2,7,9-tricarboxyl functions ionized was optimized at the HF/6-31+G(d,p) level. The electrostatic potential was calculated at the MP2/6-31+G(d,p) level using the Merz−Singh−Kollman scheme.[32] The restrained electrostatic potential (RESP) method[33] was used to fit the electrostatic potential using an atom-centered point charge model. Similar procedures were adopted to obtain the partial charges of the C5-reduced intermediates of PQQ (**II** and **III** of Scheme 1).

Substrate Preparation. As the crystal structure (1G72)[19] does not contain the substrate methanol, the latter was optimized at the HF/6-31+G(d,p) level. As per the proposal of the crystal structure,[18] the optimized methanol was docked using the SYBYL program so that the hydroxyl oxygen of methanol makes a hydrogen bond with Asp297$-CO_2^-$ and the methyl group is positioned to be proximal to the quinone carbonyl carbon C5 of PQQ in the starting structures of both A and C subunits.

Molecular Simulations. Hydrogen atoms were added to the crystal structure[19] using the program CHARMM[34] (version c27b4) and CHARMM27 all-atom force field parameters.[35] The protonation sites of histidine residues in MDH were based on the availability of proximal hydrogen bond donors and acceptors. Glu55$-CO_2$ in the heavy subunits was protonated for appropriate interactions with the carboxylate oxygen at the 2-position of cofactor. To neutralize the total charge of the enzyme, Cl^- ions were placed at a distance of 3.0 Å near the side chains of solvent-exposed Lys and Arg residues. Each complex structure with 614 crystal waters was minimized for 500 steps of steepest descent (SD) and 1500 steps of adopted basis Newton−Raphson (ABNR) methods.

The systems were solvated in an equilibrated TIP3P[36] water sphere of 42 Å radius using the center of mass of the cofactor bound to subunit A as the origin. Solvent molecules within 2.8 Å of heavy atoms were deleted. The solvated system contains the whole of subunit A and subunit B and parts of subunit C (Figure 1). The structures **A** and **B**

(27) Oubrie, A.; Dijkstra, B. W. *Protein Sci.* **2000**, *9*, 1265.
(28) Dewanti, A. R.; Duine, J. A. *Biochemistry* **2000**, *39*, 9384.
(29) Reddy, S. Y.; Mathews, F. S.; Zheng, Y.-J.; Bruice, T. C. *J. Mol. Struct.* In press.
(30) *SYBYL*, version 6.3; Tripos Associates, Inc.: St. Louis, MO.
(31) Frisch, M. J.; Trucks, G. W.; Schlegel, H. B.; Scuseria, G. E.; Robb, M. A.; Cheeseman, J. R.; Zakrzewski, V. G.; Montgomery, J. A., Jr.; Stratmann, R. E.; Burant, J. C.; Dapprich, S.; Millam, J. M.; Daniels, A. D.; Kudin, K. N.; Strain, M. C.; Farkas, O.; Tomasi, J.; Barone, V.; Cossi, M.; Cammi, R.; Mennucci, B.; Pomelli, C.; Adamo, C.; Clifford, S.; Ochterski, J.; Petersson, G. A.; Ayala, P. Y.; Cui, Q.; Morokuma, K.; Malick, D. K.; Rabuck, A. D.; Raghavachari, K.; Foresman, J. B.; Cioslowski, J.; Ortiz, J. V.; Stefanov, B. B.; Liu, G.; Liashenko, A.; Piskorz, P.; Komaromi, I.; Gomperts, R.; Martin, R. L.; Fox, D. J.; Keith, T.; Al-Laham, M. A.; Peng, C. Y.; Nanayakkara, A.; Gonzalez, C.; Challacombe, M.; Gill, P. M. W.; Johnson, B. G.; Chen, W.; Wong, M. W.; Andres, J. L.; Head-Gordon, M.; Replogle, E. S.; Pople, J. A. *Gaussian 98*, revision A.6; Gaussian, Inc.: Pittsburgh, PA, 1998.
(32) Besler, B. H.; Merz, K. M.; Kollman, P. A. *J. Comput. Chem.* **1990**, *11*, 431.
(33) Bayly, C. I.; Cieplak, P.; Cornell, W. D.; Kollman, P. A. *J. Phys. Chem.* **1993**, *97*, 10269.
(34) Brooks, B. R.; Bruccoleri, R. E.; Olason, B. D.; States, D. J.; Swaminathan, S.; Karplus, M. *J. Comput. Chem.* **1983**, *4*, 187.
(35) MacKerell, A. D., Jr.; Bashford, D.; Bellott, M.; Dunbrack, J. R. L.; Evanseck, J. D.; Field, M. J.; Fischer, S.; Gao, J.; Guo, H.; Ha, S.; Joseph-McCarthy, D.; Kuchnir, L.; Kuczera, K.; Lau, F. T. K.; Mattos, C.; Michnick, S.; Ngo, T.; Nguyen, D. T.; Prodhom, B.; Reiher, W. E. I.; Roux, B.; Schlenkrich, M.; Smith, J. C.; Stote, R.; Straub, J.; Watanabe, M.; Wiorkiewicz-Kuczera, J.; Yin, D.; Karplus, M. *J. Phys. Chem. B* **1998**, *102*, 3586.
(36) Jorgensen, W. L.; Chandrasekhar, J.; Madhura, J. D.; Impey, R. W.; Klein, M. L. *J. Chem. Phys.* **1983**, *79*, 926.

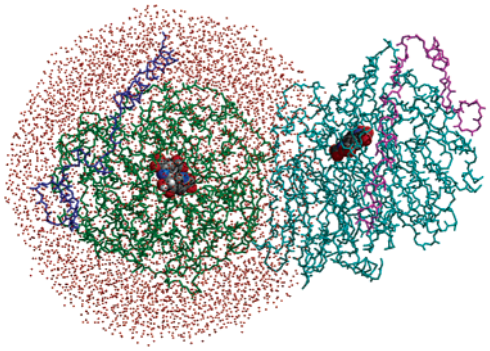

Figure 1. Stochastic boundary molecular dynamics arrangement for MDH·PQQ complex solvated in a 42 Å radius sphere of water molecules (red). Only the heavy atoms of the MDH backbone are displayed, with the four subunits in different colors. The CPK model is shown for the PQQ with hydrogens. Ions including Ca^{2+} and the hydrogens of water are not displayed.

have a total of 36 651 and 36 649 atoms, respectively, and the intermediate complexes **C** and **E** contain 36 694 and 36 766 atoms, respectively. Positions of water molecules were minimized for 200 steps of SD followed by 2000 steps of ABNR methods in each structure, keeping the ions and enzyme complex or intermediate fixed. After that, the entire system was minimized for 2000 steps by the ABNR method before starting simulations.

Stochastic boundary molecular dynamics (SBMD)[37] was carried out using the program CHARMM for 3 ns on each complex. For SBMD, a 40 Å reaction zone with a 2 Å buffer region (between 41−42 Å) from cofactor of subunit A was used. All the enzyme atoms that were at a distance beyond 42 Å from the center of mass were constrained after the minimization. Heavy atoms of the enzyme in the buffer region were constrained using force constants calculated from their average Debye−Waller factors. The system was coupled to a heat bath of 300 K with a frictional coefficient of 250 picoseconds $(ps)^{-1}$ on the heavy atoms of enzyme.[37] The frictional coefficient of buffer region water oxygens was assigned as 62 ps^{-1}.[37] A spherical boundary potential generated for a 42 Å radius sphere was used to prevent the water from "evaporating" from the surface.[38]

All atoms within 40 Å of the origin were treated by the ordinary equations of motion using verlet dynamics.[39] Atoms in the buffer zone were treated by Langevin dynamics. An integration time step of 0.0015 ps was used. SHAKE[40] was applied to all covalent bonds involving hydrogens. A constant dielectric of unity was used. Lennard−Jones interactions were truncated at a distance of 12 Å. A test simulation undertaken on structures **A** and **E** have shown that the O5 oxygen of the cofactor moves farther away from Ca^{2+} (from 2.55 to ∼3.7 Å), breaking the coordination. Therefore, during the initial period of dynamics (until 0.315 ns), a restraint of force constant 40 kcal mol^{-1} $Å^{-1}$ was imposed on the $Ca^{2+}\cdots$O5 separation in the PQQ·methanol-bound MDH simulations, **A** and **B**, while a force constant of 20 kcal mol^{-1} $Å^{-1}$ was used in complex **E**. After 0.315 nanoseconds (ns), the corresponding structures were allowed, without constraints, to rearrange according to CHARMM force field parameters.[35]

Structural Analysis. Since the active sites in both the heavy subunits of MDH are the same, the analysis was performed only on the trajectories of the first heavy subunit. The root-mean-square deviation (RMSD) values were evaluated by least-squares fitting the backbone heavy atoms of the enzyme to the minimized structure. On the basis of the stabilization of the RMSD values, MD structures were averaged during the period 2.116−3.00 ns for analysis. Structure visualization

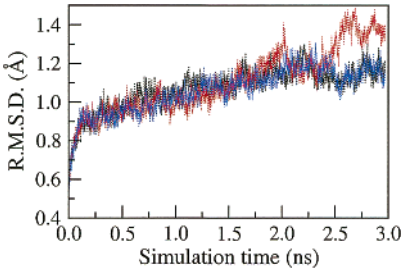

Figure 2. Root-mean-square deviations of the backbone heavy atoms of the A subunit of **A** (black), **C** (red), and **E** (blue) complexes, relative to the corresponding minimized structures during MD simulation.

of the complexes was carried out using the program gOpenMol.[41] The molecular and stereo plots were drawn using the programs MOLSCRIPT[42] rendered by Raster3D[43] and MIDAS.[44,45]

Results and Discussion

Root-Mean-Square Deviations. Figure 2 shows the time variation of RMSD with respect to the corresponding minimized X-ray structure of the backbone heavy atoms of the A subunit of complexes **A**, **C**, and **E** (Chart 1). The RMSD of the enzyme slowly increases during the course of the simulation, likely due to mobile surface residues, and stabilizes during the period 1.70−3.00 ns in structures **A** (black line) and **E** (blue line). The maximum observed RMSD values for structures **A** and **E** are 1.30 Å. The RMSD values of **C** are relatively high compared to those of structures **A** and **E**, with a maximum value of 1.44 Å (red line in Figure 2). The RMSD of the active site residues, involving cofactor, Ca^{2+}, and the enzyme residues of MDH (Glu171, Asn255, Asp297, Arg324, and Asn387) are stable, around ∼0.82 Å in the structures **A**, **C**, and **E**.

Active Site of MDH. The cofactor is involved in numerous noncovalent, mostly polar interactions in the plane of the ring.[16−19] Hydrophobic axial interactions occur above and below the cofactor plane (Figure 3). The vicinal disulfide Cys103−Cys104 located above the cofactor plane has an unusual trans configuration. It has been suggested[17,18] that the methanol substrate resides in a hydrophobic cavity bounded by Trp259, Trp531, and Leu547 residues and the disulfide Cys103−Cys104 ring. This is observed in the MD structure (Figure 3). This region in the active site is adjacent to a more polar region containing such entities as Asp297−CO_2^- and Glu171−CO_2^-.

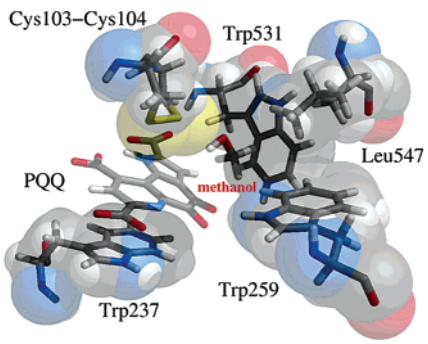

Figure 3. View of the active site comprising hydrophobic residues around the substrate methanol of the MD averaged structure **A**. Observe that the PQQ is sandwiched between the indole ring of Trp237 (below) and disulfide ring (yellow, above) in the active site of MDH.

(37) Brooks, C. L., III; Karplus, M. *J. Mol. Biol.* **1989**, *208*, 159.
(38) Brunger, A. T.; Brooks, C. L., III; Karplus, M. *Proc. Natl. Acad. Sci. U.S.A.* **1985**, *82*, 8458.
(39) Verlet, L. *Phys. Rev.* **1967**, *159*, 98.
(40) Ryckaert, J. P.; Ciccotti, G.; Berendsen, H. J. C. *J. Comput. Phys.* **1977**, *23*, 327.
(41) Laaksonen, L. *gOpenMol, A graphics program for the analysis and display of molecular dynamics trajectories*; version 2.10, 1992; Vol. 10, p 33.

Table 1. Nonbonded Distances (Å) between the Substrate Methanol and Other Atoms in the Active Site and Their Standard Deviations (in Parentheses) of the MD Averaged (2.116−3.0 ns) Structures

nonbonded distances	A	B
OD1(Asp297)···O(methanol)	5.54 (±0.62)	3.39 (±0.38)
OD1(Asp297)···H(methanol)	5.33 (±0.77)	3.34 (±0.74)
OD2(Asp297)···O(methanol)	6.76 (±0.38)	3.14 (±0.45)
OE1(Glu171)···O(methanol)	2.79 (±0.15)	3.20 (±0.15)
OE1(Glu171)···H(methanol)	1.88 (±0.20)	3.87 (±0.18)
Ca^{2+}···O(methanol)	4.48 (±0.19)	2.43 (±0.15)
C5···C(methanol)	3.77 (±0.29)	3.54 (±0.16)
C5···HC1(methanol)	3.71 (±0.72)	3.81 (±0.63)
C5···HC2(methanol)	3.70 (±0.73)	3.81 (±0.65)
C5···HC3(methanol)	3.68 (±0.72)	3.83 (±0.64)
C5···O(methanol)	4.59 (±0.26)	3.21 (±0.16)
O5···O(methanol)	4.79 (±0.29)	2.71 (±0.18)
O5···H(methanol)	4.51 (±0.31)	1.98 (±0.53)
O(Wat1)···O(methanol)	4.87 (±0.86)	3.01 (±0.17)
O(Wat1)···C(methanol)	4.34 (±0.89)	4.34 (±0.17)
O(Wat1)···HC1(methanol)	4.34 (±1.15)	4.83 (±0.27)
O(Wat1)···HC2(methanol)	4.37 (±1.10)	4.82 (±0.26)
O(Wat1)···HC3(methanol)	4.34 (±1.15)	4.82 (±0.28)

It has been proposed that the residues Asp297 and Arg324 and crystal water play essential roles in methanol oxidation by PQQ.[16−19] Each heavy subunit contains Ca^{2+}, which assists in holding reactants in position. The X-ray structures indicate hexacoordination of the Ca^{2+} ion, with three of its six ligands belonging to the cofactor. These are the C5 quinone carbonyl oxygen O5, pyridine nitrogen N6, and C7 carboxylate oxygen O7A.[16−19] The other three ligands to Ca^{2+} are the carboxylate oxygens of Glu171 and the amide oxygen of Asn255.

The nonbonded distances of various atoms of the active site of MD (and their standard deviations averaged for the time period 2.116−3.00 ns) as well as the X-ray structures involving methanol and Ca^{2+} are given in Tables 1 and 2, respectively. An overview of the active site of structures **A**−**E** (Chart 1) is given in Figure 4. The stereo plots of mechanistically significant positions of structures **A** and **E** are given in Figure 5.

Interactions with Methanol Substrate. The hydride transfer mechanism of methanol oxidation by MDH (Scheme 1) has been proposed to take place by Asp297−CO_2^- general base abstraction of the proton from the hydroxyl group of methanol.[17,18] This feature has been suggested from the results of docking studies of methanol in the active site of MDH.[46] However, from our MD studies, this does not appear to be likely. A time variation plot of separation of OD1(Asp297)···O(methanol) in structure **A** shows that the methanol oxygen is not close to the carboxylate oxygen, OD1 of Asp297 (Figure 6a). Indeed, after 0.125 ns of dynamics, the methanol oxygen remains at an average distance of 5.54 ± 0.62 Å from OD1 of Asp297 (Table 1). The methanol oxygen is located at a distance 4.48 ± 0.19 Å from Ca^{2+} during dynamics. After 0.125 ns, the methanol oxygen forms a hydrogen bond (2.79 ± 0.16 Å) with the carboxylate oxygen (OE1) of Glu171−CO_2^-, which remains during the remainder of the simulation (Figure 6b). Thus, Glu171−CO_2^- is positioned to play the vital role of general base to abstract the hydroxyl hydrogen of methanol.

Chemical studies have established that the C5 carbonyl of PQQ is more reactive than the C4 carbonyl in addition reactions in solution with methanol, acetone, cyanate,[22] and also amines.[10,11] Significantly, during most of the simulation, the methanol carbon approaches C5 of PQQ (3.77 ± 0.29 Å) sufficiently for hydride transfer (Table 1 and Figure 6c).

A few sharp peaks noticed in Figure 6, around 1.90 and 2.07 ns, show dissociation of methanol from Glu171−CO_2^- (7.9 Å), and their study provides in retrograde the channel for substrate entrance (Figure 7). During this period, the methanol oxygen forms a hydrogen bond (2.70 Å) with the backbone carbonyl oxygen of Cys103. The position of the Cys103−Cys104 disulfide is likely to hold the substrate at the entrance of the active site, besides acting as a shield from bulk waters. This orientation of methanol is stabilized by proximal surface waters. Interestingly, this is the likely channel that methanol follows to enter the active site.

From a comparison of the simulations of structures **A** and **B** (Figure 4), it can be seen that protonation of OD2 of Asp297−CO_2^- in structure **B** influences methanol orientation. Inspection of the average values (Table 1) reveals that the methanol substrate is oriented in such a fashion that the reaction could not occur. Thus, structure **B** cannot be involved in the catalytic mechanism and is henceforth disregarded in the following sections.

Coordination of Calcium Ion. The coordination of Ca^{2+} is altered during MD simulation. In structure **A**, the average separations from Ca^{2+} to the N6 and O7A of PQQ are 2.39 and 2.15 Å, respectively. The distances from Ca^{2+} to the carboxylate oxygens (OE1 and OE2) of Glu171 and the side chain amide oxygen (OD1) of Asn255 of MDH are 2.21, 2.19, and 2.26 Å, respectively (Table 2). When the restraint on separation between the carbonyl oxygen O5 of PQQ and Ca^{2+} is removed at 0.315 ps, the distance increases to 3.35 ± 0.19 Å and remains so (black line of Figure 8). However, crystal water Wat1 coordinates to Ca^{2+} (2.24 ± 0.08 Å) retaining hexacoordination of Ca^{2+} in structure **A** (Figure 5A). This is unlike that observed in the MDH·PQQ crystal structure, where Wat1 is 3.53 Å from Ca^{2+}. Such differences between the experimental

Table 2. Nonbonded Distances (Å) between Ca^{2+} and Other Atoms in the Active Site and Their Standard Deviations (in Parentheses) of the MD Averaged (2.116−3.0 ns) and X-ray Structures

nonbonded distances	X-ray	A	B	C	E
O5···Ca^{2+}	2.55	3.35 (±0.19)	3.65 (±0.11)	2.03 (±0.03)	3.46 (±0.24)
N6···Ca^{2+}	2.61	2.39 (±0.11)[c]	2.45 (±0.09)[c]	2.29 (±0.06)[d]	2.35 (±0.07)[d]
O7A···Ca^{2+}	2.70	2.15 (±0.06)	2.13 (±0.05)	3.54 (±0.13)	2.18 (±0.07)
OE1(Glu171)···Ca^{2+}	2.62	2.21 (±0.07)[d]	2.21 (±0.07)[d]	3.76 (±0.15)	2.26 (±0.08)[d]
OE2(Glu171)···Ca^{2+}	2.53	2.19 (±0.06)[d]	2.16 (±0.06)[d]	2.32 (±0.10)[c]	2.21 (±0.07)[d]
OD1(Asn255)···Ca^{2+}	2.82	2.26 (±0.08)	2.31 (±0.11)	3.98 (±0.22)	2.38 (±0.15)[d]
O(Wat1)···Ca^{2+}	3.53	2.24 (±0.08)	2.27 (±0.08)	2.26 (±0.06)[a]	2.35 (±0.09)
OD1(Asp297)···Ca^{2+}	4.29	4.84 (±0.21)[b]	4.00 (±0.30)[d]	2.21 (±0.07)	2.14 (±0.05)
OD2(Asp297)···Ca^{2+}	3.38	4.56 (±0.29)[b]	4.52 (±0.28)	2.23 (±0.08)	3.56 (±0.12)[c]

[a] Wat91 instead of Wat1. [b] Value averaged during 2.116−2.70 ns [c] Values within 0.25 Å variation from the crystal structure. [d] Values within 0.26−0.45 Å variation from the crystal structure.

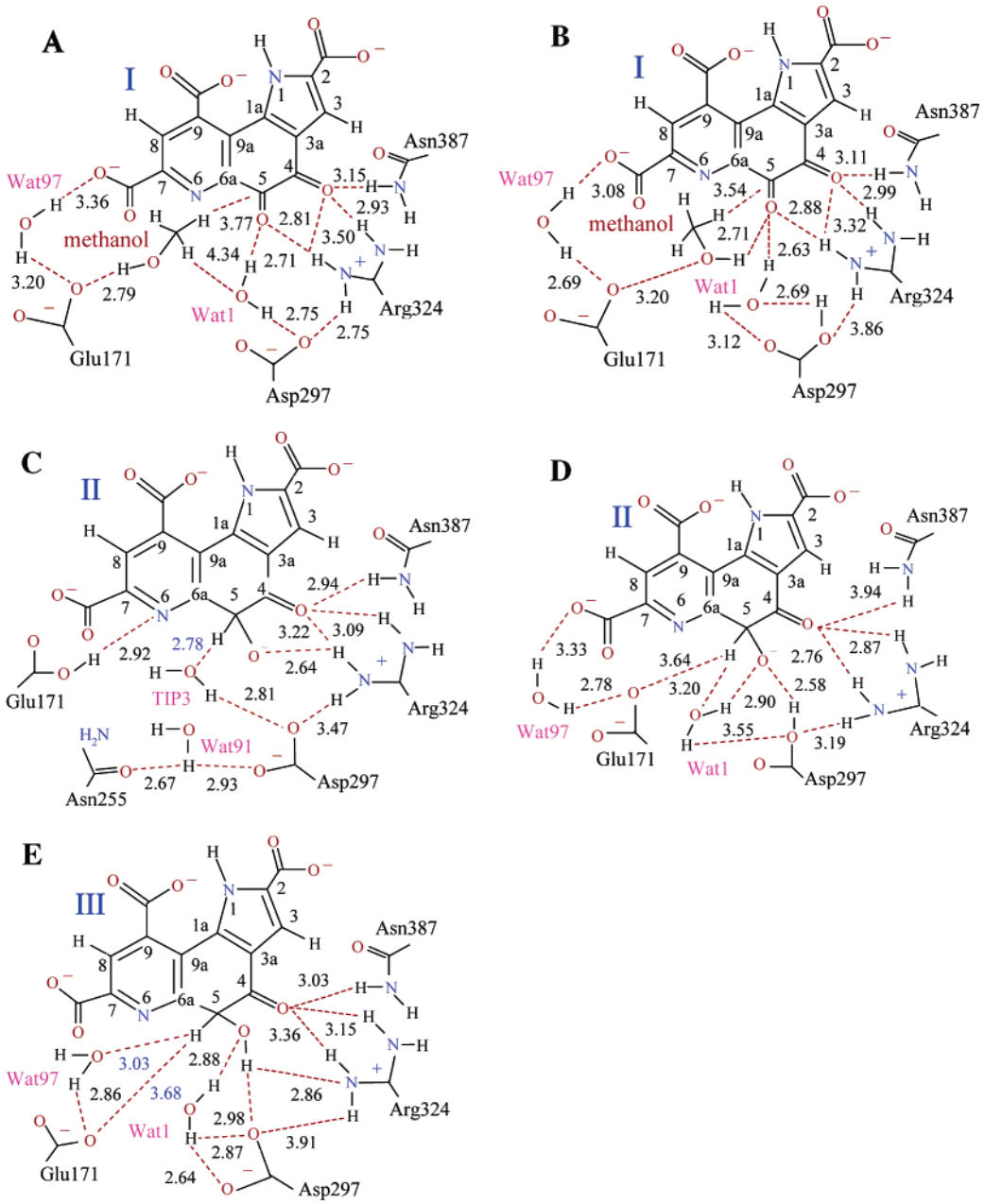

Figure 4. Active site residues related to hydride transfer mechanism of the methanol oxidation by MDH in structures **A**−**E**. Ca^{2+} is omitted for clarity. Nonbonded interactions are in red, and distances (Å) between the heavy atoms are given in black. The separation between H (at C5 of cofactor) and O in structures **C** and **E** are in blue.

and simulated coordination patterns of Ca^{2+} have been observed in the MD studies on calbindin.[47−49] Besides, the carboxylate oxygen OD1 of Asp297 approaches Ca^{2+} (∼2.2 Å) after 2.70 ns, altering the coordination of Ca^{2+}.

The pH optimum for enzyme activity is 9 such that both Glu171 and Asp297 of MDH are expected to be carboxylates. Thus, structures **C** and **D** could only be present as transient structures, after departure of formaldehyde. Protonation of one of the carboxylate oxygens (OE1) of Glu171 in complex **C** disrupts the coordination of Ca^{2+} with the carboxylate oxygen (OE1) of Glu171, amide oxygen of Asn255, and C7 carboxylate oxygen O7A of **II**, while the coordination to oxyanion O5 (red line of Figure 8) and pyridine nitrogen N6 of **II** are unaffected. However, hexacoordination of Ca^{2+} is retained during simulation by coordination with crystal water Wat91 and both carboxylate oxygens of Asp297−CO_2^- (Table 2).

In complex **E**, the Ca^{2+} is coordinated with the N6 and O7A of **III**, as well as both carboxylate oxygens of Glu171−CO_2^- and the amide oxygen of Asn255 (Table 2). Similar to the feature observed in the simulation of structure **A**, the separation between Ca^{2+} and the O5 hydroxyl oxygen of **III** after 0.725 ns fluctuates (blue line of Figure 8) with an average value 3.46 ± 0.24 Å (Table 2). Besides, the crystal water Wat1 is coordinated to Ca^{2+}, with an average separation of 2.35 ± 0.09 Å. One of the carboxylate oxygens (OD1) of Asp297−CO_2^- also coordinates to Ca^{2+} (2.14 ± 0.05 Å) resulting in heptaco-

(42) Kraulis, P. J. *J. Appl. Crystallogr.* **1991**, *24*, 946.
(43) Merritt, E. A.; Bacon, J. D. *Methods Enzymol.* **1997**, *277*, 505.
(44) Ferrin, T. E.; Huang, C. C.; Jarvis, L. E.; Langridge, R. *J. Mol. Graphics* **1988**, *6*, 13.
(45) Huang, C. C.; Pettersen, E. F.; Klein, T. E.; Ferrin, T. E.; Langridge, R. *J. Mol. Graphics* **1991**, *9*, 230.

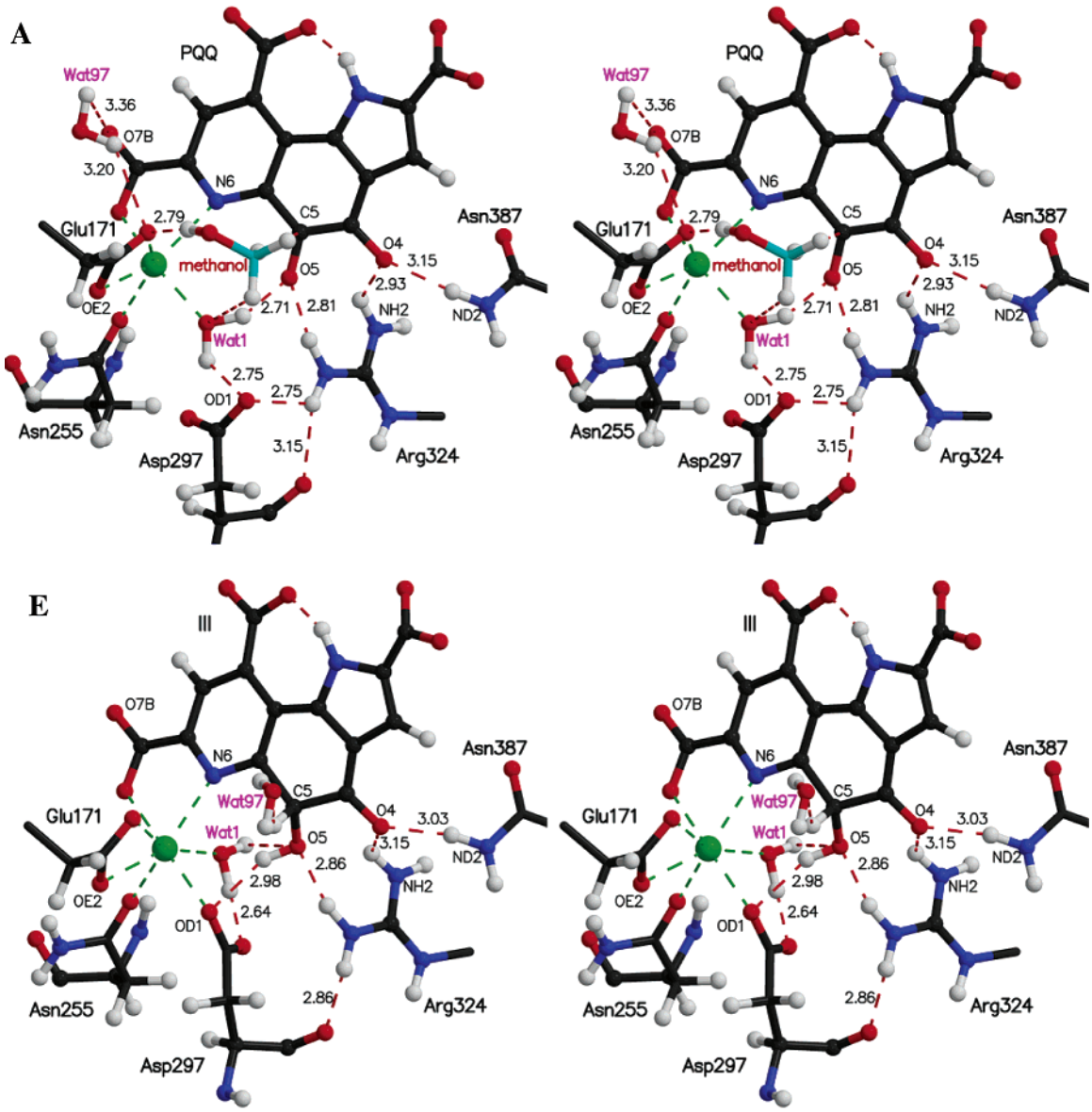

Figure 5. Stereoview of the active site depicting Ca^{2+} coordination and interactions of Glu171, Asp297, Arg324, and Wat1 in the MD averaged (2.116−3.0 ns) structures **A** and **E**, expected at pH 9. The methanol carbon in **A** is colored cyan. The Ca^{2+} coordination is in green, and coordinating distances are omitted for clarity and given in Table 2. Nonbonded interactions are shown in red. Average nonbonded distances between heavy atoms are given in Å.

ordination of Ca^{2+} (Figure 5E). A change in coordination pattern of Ca^{2+} has been observed in the crystal structure of a mutant MDH.[21]

Role of Asp297. Asp297−CO_2^- has been suggested[17,18] to assist as a general base in the migration of the H5 hydrogen of **III** to provide the hydroquinone $PQQH_2$ (Scheme 1). Besides coordination to Ca^{2+}, OD1 of Asp297 is preoccupied in hydrogen bond interactions with the O5 hydroxyl oxygen of **III** and crystal water Wat1 (Tables S1 and S2, Supporting Information). The average separations of OD1 of Asp297−CO_2^- from C5 and H5 are 3.74 ± 0.22 and 3.43 ± 0.44 Å, respectively. The distance of OD2 of Asp297 from H5 hydrogen at C5 is greater than that to the other carboxylate oxygen OD1. Time variation plot of the separation of carboxylate oxygen OD1 of Asp297−CO_2^- and H5 (Figure S1a, Supporting Information) of structure **E** shows occurrence of 0.9 mol % conformers with values less than 2.7 Å, and Asp297−CO_2^- likely has the ability to interact with H5 at C5.

Interactions with Arg324. Interaction of Arg324, as well as Ca^{2+} with the carbonyl oxygen of C5 of PQQ, would be expected to assist hydride addition. In complex **A**, the heavy atom distance of the hydrogen bond between the guanido NH1−HH11 of Arg324 and carbonyl oxygen O5 of PQQ is 2.81 ± 0.14 Å (Figure 5A). This is consistent with the crystal structure data.[18,19] NH1−HH11 of Arg324 also engages in a favorable hydrogen bond interaction with the carboxylate oxygen (OD1) of Asp297−CO_2^- (2.75 ± 0.16 Å), while the NH1−HH12 links to the backbone carbonyl oxygen of Asp297 (3.15 ± 0.27 Å). The guanido group NH2−HH22 of Arg324 forms a stable hydrogen bond with the carbonyl oxygen O4 of PQQ (2.93 ± 0.18 Å). Similar interactions with Arg324 are present in structure

(46) Keitel, T.; Diehl, A.; Knaute, T.; Stezowski, J. J.; Höhne, W.; Görisch, H. *J. Mol. Biol.* **2000**, *297*, 961.
(47) Mehler, E. L.; Kushick, J. N.; Weinstein, H. *Mol. Simulation* **1993**, *10*, 309.
(48) Ahlstorm, P.; Teleman, O.; Kordel, J.; Forsen, S.; Jonsson, B. A. *Biochemistry* **1989**, *28*, 3205.
(49) Marchand, S.; Roux, B. *Proteins: Struct., Funct. Genet.* **1998**, *33*, 265.

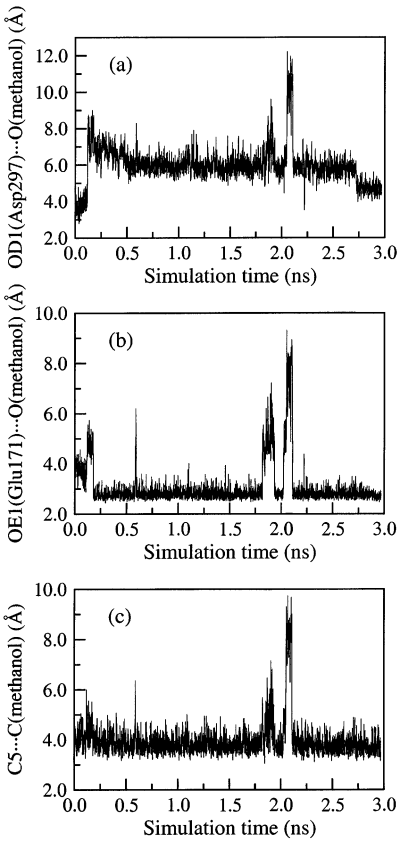

Figure 6. Time-dependent variation of the distance between (a) the carboxylate oxygen (OD1) of Asp297−CO_2^- and the methanol oxygen, (b) the carboxylate oxygen (OE1) of Glu171−CO_2^- and the methanol oxygen, and (c) C5 of PQQ and the methanol carbon of complex **A**.

C (Figure 4C). However, the separation between the guanido NH1 of Arg324 and carboxylate oxygen (OD1) of Asp297−CO_2^- is large (3.47 ± 0.21 Å).

In complex **E**, a hydrogen bond interaction (2.86 ± 0.16 Å) is observed between the guanido NH1 of Arg324 and the O5 oxygen of **III** after 0.15 ns (Figure 5E). During the entire simulation, a favorable interaction between the NH1−HH11-(Arg324) and carbonyl oxygen of Asp297 is present, while the hydrogen bond between NH1−HH12(Arg324) and the carboxylate oxygen (OD1) of Asp297−CO_2^- is not present after 0.15 ns. The guanido nitrogen NH2 of Arg324 forms a hydrogen bond, at an average distance of 3.15 ± 0.33 Å, with the C4 carbonyl oxygen O4 of **III** (Figure 4E).

Motions of Crystal Waters. Besides the hydrophobic residues around PQQ and methanol seen in Figure 3, the active site of MDH has many polar residues. There are seven crystal waters in proximity to PQQ in the MD averaged structure **A** (Figure 9). During the entire simulation, the crystal water Wat1 in structure **A** forms strong hydrogen bonds with the carbonyl oxygen O5 of PQQ and the carboxylate oxygen OD1 of Asp297−CO_2^- (Figure 5A). Five of the other crystal waters, Wat63 to Wat66 and Wat97, form a cluster (upper left of Figure 9) above the PQQ plane. One of these, Wat65, is linked to the backbone nitrogen of Cys104 and carbonyl oxygen of Asp105 (Table S2, Supporting Information). Wat97 forms a hydrogen bond with one of the carboxylate oxygens (OE1) of Glu171. Wat91 stands away from other water molecules and lies below the PQQ plane. The same water forms hydrogen bonds with the C7 carboxylate oxygen O7A of PQQ and also with the hydroxyl oxygen of Thr235, amide oxygen, and backbone nitrogen of Asn255. A few other crystal waters also stabilize enzyme residues, which have a role in catalysis. Of interest is the link of Wat124 to the guanido nitrogen (NH2) of Arg324.

In complex **C**, the crystal water Wat91 replaces Wat1 during the course of dynamics, with the latter moving farther away from the active site after 0.1 ns of simulation (Figure 4C). Distinctly, Wat91 forms a hydrogen bond with the carboxylate oxygen (OD2) of Asp297−CO_2^-, amide oxygen of Asn255, and O7A of the cofactor (Table S2, Supporting Information). In structure **E**, Wat1 is hydrogen bonded to the hydroxyl oxygen O5 of **III**, in good agreement with the crystal structure of

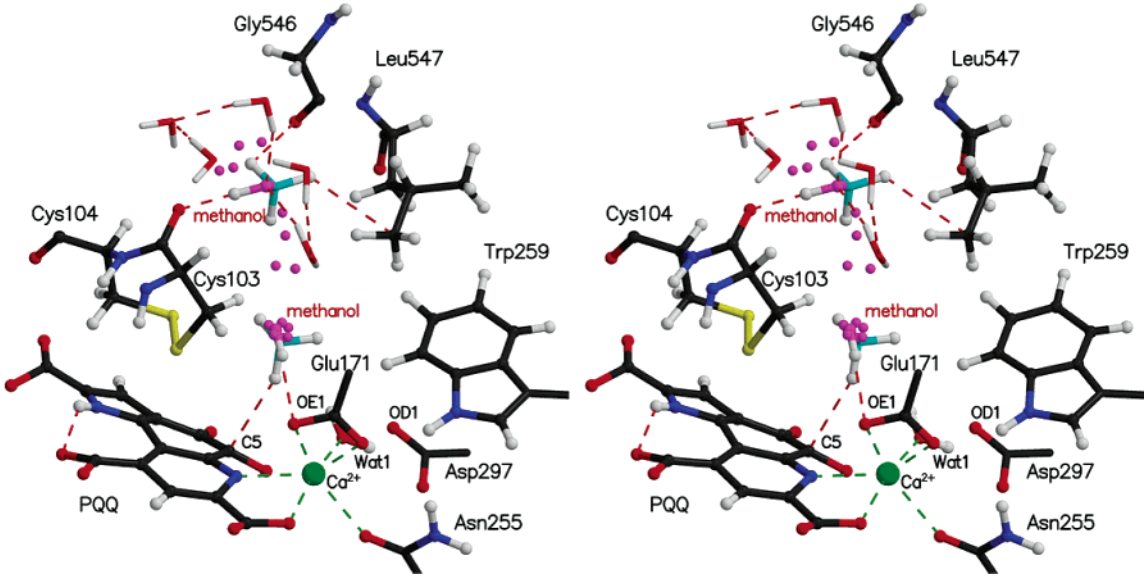

Figure 7. Stereoview of the MD snapshot at 2.07 ns, depicting the path of methanol into the active site of structure **A**. The Ca^{2+} coordination is in green, and nonbonded interactions are in red. The methanol carbons and oxygens are colored cyan and magenta, respectively. The trace of methanol oxygen (magenta dots) corresponds to MD snapshots during the period 2.07−2.15 ns. Notice that the methanol on the surface (at 2.07 ns), amidst TIP3P waters, interacts with Cys103. But at 2.10 ns, methanol flips to be at the center of the active site. Also, notice that the methanol makes interactions with the Glu171−CO_2^- and C5 of PQQ (at 2.12 ns).

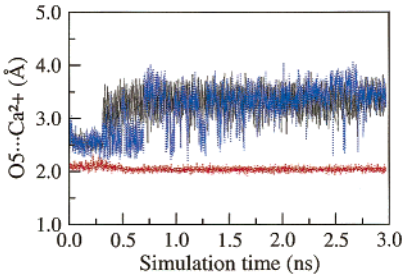

Figure 8. Time-dependent variation of the distance between cofactor oxygen O5 and Ca^{2+} of MD simulated complexes **A** (black), **C** (red), and **E** (blue).

MDH−PQQ.[19] Wat1 also forms hydrogen bonds with both carboxylate oxygens of Asp297−CO_2^- (Figure 4E). A significant feature is the position of Wat97 that is located intermediate to Glu171−CO_2^- and C5 of **III**. Other crystal waters are similarly arranged as in structure **A**, though wide fluctuations are noticed in certain separations (like Wat91 to the indole nitrogen (NE1) of Trp237) in structures C and **D** (Table S2, Supporting Information).

Interactions of a Particular TIP3P Water and Glu171. The residues Met102, Cys103−Cys104, Asp105, Trp531, and Leu547 are located at the surface of the enzyme active site. In structure **A**, no TIP3P water enters the active site. During simulation of complex **C**, a TIP3P water penetrates into the active site and, after 0.85 ns, is proximal (2.78 ± 0.29 Å) to H5 at tetrahedral C5 of **II** (Figure 4C). The same water forms a hydrogen bond with the carboxylate oxygen (OD1) of Asp297−CO_2^- and is proximal to the ring carbon, CH2 of Trp531 (Table S2, Supporting Information).

In complex **E**, the mole percentage of conformational isomers in which Glu171−CO_2^-···H−C5 of **III** is ≤2.7 Å is 0.075 mol % (Figure S1b, Supporting Information). The average distance between this carboxylate oxygen and H5 is 3.68 ± 0.26 Å. Thus, the positioning of Glu171−CO_2^- to assist in proton isomerization to provide $PQQH_2$ is rare. The penetration of a TIP3P water

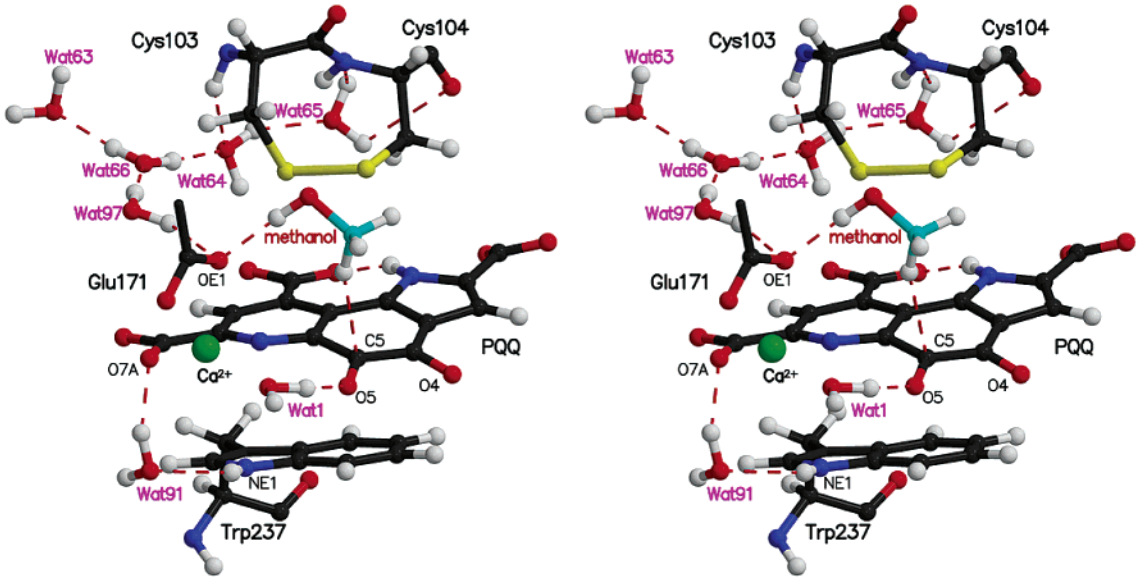

Figure 9. Stereoview of the active site of the MD averaged structure **A** showing positions of crystal waters. The methanol carbon is colored cyan, and Ca^{2+} is colored green. Nonbonded interactions are shown in red. Notice that the peptide bond of vicinal disulfide (yellow) has trans configuration.

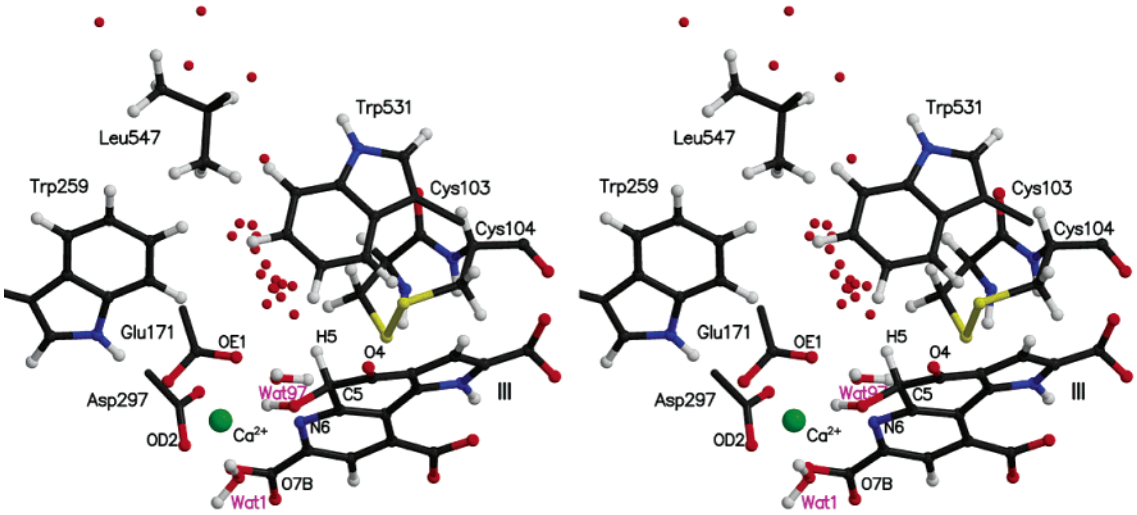

Figure 10. Stereoview of the trail of a TIP3P water oxygen (red) entering the active site of the MD averaged (from 0.9 to 2.0 ns) structure **E**. Snapshots of TIP3P oxygen at 0.075, 0.078, 0.081, 0.084, 0.087, 0.135, 0.27, 0.45, 0.63, 0.81, 0.99, 1.17. 1.35, 1.53, 1.71, 1.89, 1.923, 1.959, 1.975, and 1.996 ns are shown. Notice that the path of TIP3P leads to the H5 at C5 of **III** and carboxylate oxygen of Glu171.

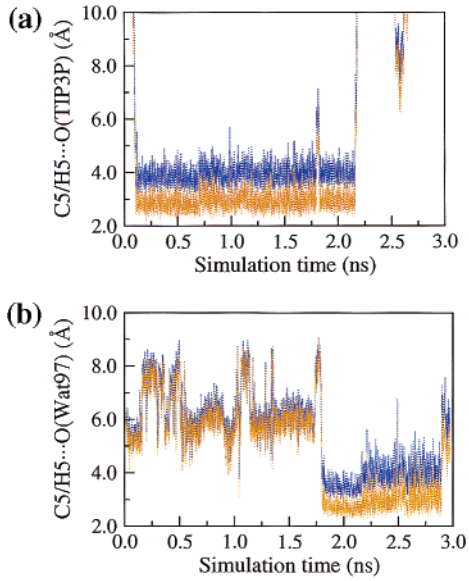

Figure 11. Time-dependent variation of separations of C5 (blue) and H5 (yellow) of **III** with the (a) TIP3P water and (b) crystal water Wat97 oxygens of structure **E**.

into the active site is shown in Figure 10. Initially, the TIP3P water that is followed is at a distance of 24 Å from H5 and then, after 0.135 ns of dynamics, enters the active site and gradually approaches and remains proximal to the H5 at C5 (3.01 ± 0.44 Å) until 2.155 ns (Figure 11a). Significantly during that period, the same TIP3P water forms a hydrogen bond with the carboxylate oxygen (OE1) of Glu171−CO_2^- (2.82 ± 0.43 Å). The TIP3P water gradually drifts away from the active site after 2.15 ns. During the period 2.155−2.890 ns, crystal water Wat97, instead of a TIP3P water, is proximal to the H5 of **III** (Figure 11b) and Glu171−CO_2^-.

At 2.90 ns, another TIP3P water enters the active site to replace Wat97. This suggests that a Glu171−CO_2^-···H_2O···H−C5 relay is involved in abstraction of the C5 hydrogen of **III**. This is an interesting feature not suggested by the X-ray studies.[16−19] The water channel, so discovered, may also serve as a path to allow ammonia and other small molecules, which can act as promoters[21] to catalysis, to enter the active site. Interestingly, this feature is in accord with speculation that ammonium might be positioned near Glu171.[50]

Other Interactions of PQQ. Besides the interactions of the PQQ with Glu171, Asp297, Arg324, and crystal waters mentioned in the earlier sections, there is a network of hydrogen bond interactions and salt bridges that involve PQQ in structure **A**. A hydrogen bond interaction between the amide side-chain of Asn387 and carbonyl oxygen at C4 of PQQ occurs in the MD averaged structures (Table S1, Supporting Information). As seen in Table S3 (Supporting Information), most of the nonbonded separations related to the 2, 7, and 9 carboxylate oxygens of PQQ of the MD structure are consistent with the crystal structure[19] and MD studies[29] and henceforth not discussed here. Similar features are also observed in the MD simulation of structures of **C** and **E**. In structure **C**, a strong hydrogen bond is observed between the pyridine nitrogen, N6, and Glu171−CO_2H (Figure 4C).

(50) Hothi, P.; Basran, J.; Sutcliffe, M. J.; Scrutton, N. S. *Biochemistry* **2003**, *42*, 3966.

Chart 2

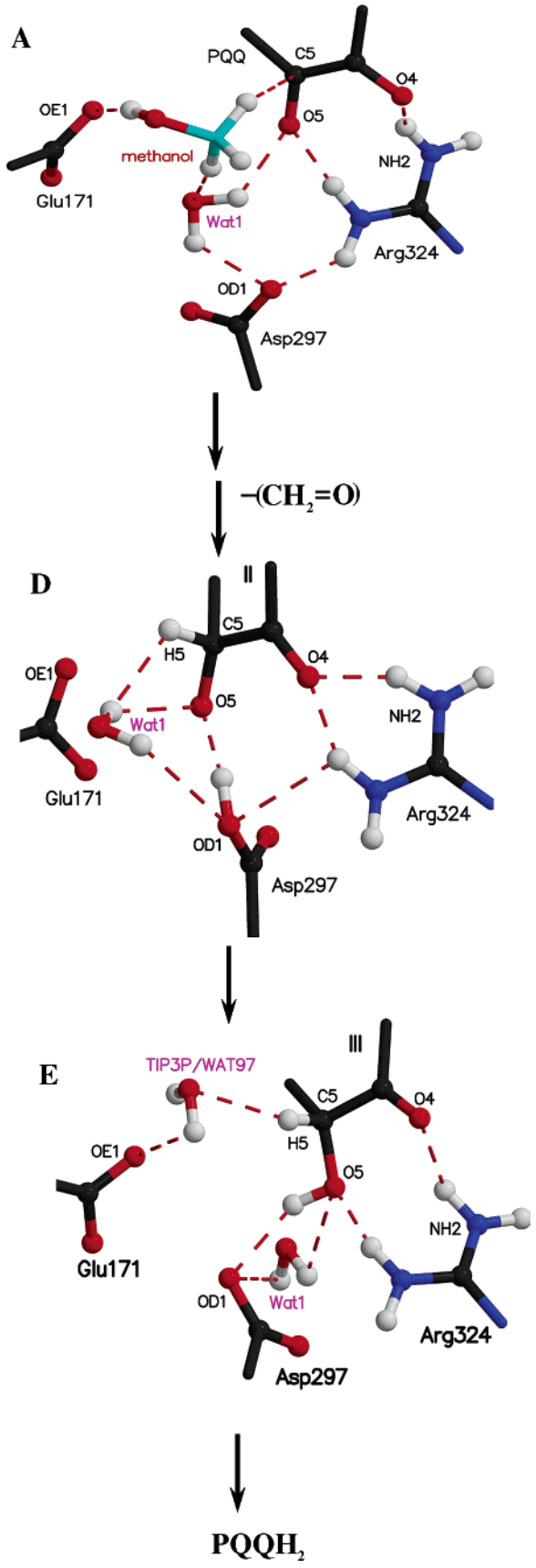

Conclusions

Information concerning the stepwise mechanism of MDH·PQQ oxidation of methanol are provided by the MD simulations

of the current and previous[29] studies. On the basis of the X-ray structure of **II** (Scheme 1) in PQQ oxidation of methanol, the mechanism involves hydride equivalent transfer from the substrate methanol to the C5 quinone carbonyl carbon of PQQ.[19] The structure of the methanol complex has not been previously determined. Mechanisms involving general base-catalyzed proton ionization of the methanol substrate and concerted hydride transfer must be considered. In structure **A**, Glu171$-CO_2^-$ is at an average distance of 2.23 Å from $H-OCH_3$. Further, $HO-CH_2-H$ is as close as 3.01 Å to the C5 of PQQ. This geometry and increase of quinone oxidation potential by hydrogen bonding of C5═O and C4═O of PQQ with Arg324 allows a concerted reaction. So Glu171$-CO_2^-$, rather than the suggested[16−19] Asp297$-CO_2^-$, is most likely the general base catalyst.

The structures related to mechanistic steps of methanol oxidation of the enzyme are given in Chart 2. The immediate product from methanol oxidation is formaldehyde. The means of departure of CH_2O is unknown. It is possible that the formaldehyde product interacts with one of the many waters in the active site vicinity to form the stable hydrate $CH_2(OH)_2$. Hydride transfer to −C5(═O)− of PQQ leads to $-(H)C5(O^-)-$ of **II**. The structure **B** can be dismissed on the basis that the positioning of methanol provides no means for its oxidation by PQQ. The formation and lifetime of $-(H)C5(O^-)-$ of **II** are stabilized by hydrogen bonding to Arg324 as can be seen in structure **C**. In structure **D**, the average distance from the oxyanion of $--(H)C5(O^-)-$ and the protonated carboxylate oxygen of Asp297$-CO_2H$ is 2.58 Å, indicating a strong hydrogen bond.[29] Thus, protonation of the $-(H)C5(O^-)-$ entity of **II** is likely to occur via the Asp297$-CO_2H$ of transient structure **D**. The MD simulation of the structure **E** suggests that Glu171$-CO_2^-$ is most probably, through a water molecule (either TIP3P or Wat97), involved in the isomerization of **III** to provide the hydroquinone $PQQH_2$. This isomerization is made easy by the gain in resonance energy from aromatization. The reaction is assisted by the hydrogen bonding of Arg324 to both $-(H)C5(OH)-$ and C4═O oxygens. The channel for diffusion of substrate and water molecules into the active site has been traced, and the possibility that a promoter catalyst can enter the active site in the same manner has been considered. Our results indicate that Glu171 is particularly vital in the enzyme mechanism, and we suggest mutational and solvent isotope effect studies to test our hypothesis.

Acknowledgment. We thank Dr. Ya-Jun Zheng for suggestions. The work was supported by funds from the NIH (5R37DK0917136). The authors acknowledge computer time on UCSB's SGI Origin 2000 and at NPACI, San Diego Supercomputer Center.

Supporting Information Available: Tables S1, S2, and S3 (nonbonded distances (Å) of the active site residues of the X-ray and MD averaged structures) and Figure S1 (time-dependent variation of separations of the C5 (blue) and H5 (yellow) of **III** with the carboxylate oxygens (a) OD1 of Asp297 and (b) OE1 of Glu171 in complex **E**). This material is available free of charge via the Internet at http://pubs.acs.org.

JA034406Y